Journal of Applied Polymer Science

Facile preparation of asymmetric Ni/PVC film with controlled structure: Application as a high-performance EMI shielding material

Yang Zhang, Xiaoxia Fang, Bianying Wen, Wenqi Zou
Department of Material Science and Engineering, Beijing Technology and Business University, Beijing 100048, China
Correspondence to: B. Wen (E-mail: wenbianying@tsinghua.org.cn)

ABSTRACT: Controlling the spatial configuration of conductive fillers in thin composites by a facile strategy is critical to widely commercial use these materials for electromagnetic interference (EMI) shielding applications. In this work, a series of free-standing thin Ni/polyvinyl chloride (PVC) films with the same composition just systematically varied Ni particles dispersion states was prepared by solution casting method. The relationships between the structure and properties were also investigated. Ni particles motion was governed by evaporation and sedimentation during solvent evaporation with the presence of soluble PVC influencing the casting solution viscosity. The experimental results fit the 1D model. In dilute casting system, the effective concentration of Ni particles in the lower part of the film was significantly enhanced and a dense, closed packed conductive network was formed. This special distribution of Ni particles was found to play a key role in the corresponding properties. Compared to the uniform film, the film which was fabricated from the casting solution containing 0.03 g/mL PVC, exhibited much better electrical conductivity and EMI shielding performance. Furthermore, the detailed study shows that the obtained thin film exhibited excellent EMI SE values per unit film thickness of 200 dB/mm. Meanwhile, the resultant films possessed thermal conductivity of 0.32∼0.59 W/(m·K) depended on whether a Ni continuous network formation throughout the whole film in the temperature range of 30∼60°C. Our study results pave thus the way for scalable fabrication of substrate-free systems that have advantages in multifunctional complex devices. © 2015 Wiley Periodicals, Inc. J. Appl. Polym. Sci. **2015**, *132*, 42560.

KEYWORDS: composites; conducting polymers; films; magnetism and magnetic properties; structure–property relations

Received 14 March 2015; accepted 31 May 2015
DOI: 10.1002/app.42560

INTRODUCTION

Recently, exponential increase in electromagnetic radiations from electronic devices has led to a new kind of problem as electromagnetic pollution. It is essential to maintain the functionality and integrity of electronic devices by attenuating of electromagnetic interference (EMI). The EMI continues to be a more serious concern in modern society. An effective method to reduce or suppress EMI is by using EMI shielding materials. Compared with traditional metal-based EMI shielding materials, conductive fillers/polymer composites are more attractive due to their cost effectiveness, excellent processability, flexibility, and broad shielding bandwidth.[1–5] These unique features offer great promise for usage in EMI shielding industry. The EMI shielding efficiency (SE) of a polymeric composite depends on many factors, including the filler dispersion state,[6–8] characteristics of each component,[9] composition,[10,11] and thickness.[12] The EMI SE can be enhanced by increasing the thickness and/or the filler content. But these factors increase the cost and limit its scalability. In addition, the thick composites make them inconvenient for the application in some special fields such as aerospace, microelectronics, and weapon equipment.

Generally, the conductive fillers form a continuous network path in composites above a critical concentration, which strongly depends on the filler dispersion state.[13–17] According to electromagnetic transmission line theory, materials with higher electrical conductivity have higher SE. As for a constant composition or thickness, technological control the fillers spatial distribution throughout the composite could enhance the filler effective concentration to obtain high EMI shielding performance materials. In addition, other properties (such as the thermal conductivity) of resultant composites are also influenced by the filler distribution. But the critical challenge is how to obtain and/or enhance a certain spatial dispersion of fillers in polymer matrix during manufacturing process. To date, diverse techniques have been developed to adjust the fillers spatial distribution in composites, including layer-by-layer method,[18]

Additional Supporting Information may be found in the online version of this article.

electrophoretic deposition,[19] layer-multiplying coextrusion,[20] and under external force field.[21] While the need of complex fabrication techniques, special conditions or instruments, such as centrifugation, electrodes, layer-multiplying coextrusion system or external magnetic field, limits the widely commercial use of resulting composites. Moreover, the potential for future industrial application demands large-scale production. Therefore, innovation in relative thin polymeric composites with controllable filler distribution via a facile and large-scale approach has been an urgent challenge to be addressed.

Since the thickness could be well controlled by adjusting the volume and concentration of the suspension, combined with no special conditions or post-drying process are needed, these distinct advantages make solution casting as a convenient and cost-effective approach to fabricate thin films. Many researchers have reported the EMI shielding properties of various polymer composites using solution casting technology. For instance, Liang *et al.*[22] reported the EMI SE of ~21 dB for the solution-casted graphene/epoxy composites at 15 wt % loading of reduced graphene sheets. Liu *et al.*[10] prepared well-dispersed SWCNT/PU films using a solution blending method. An EMI SE up to 17 dB was obtained for the 2 mm thick film with 20 wt % SWCNT loading. However, in many previous researches, how to control the spatial configuration of conductive fillers in solution-casted composite was always neglected.

When a liquid film solidifies during drying, the concentration of particles increases over time. The structure of resultant film may be different from expectations derived from original composition of the suspension.[23,24] In recent years, some studies have been conducted to describe monodispersed silica particles distribution in films for water-soluble system.[25,26] Their results showed that the particles distribution was influenced by evaporation, sedimentation, and diffusion. The balance between these three motions determines particles arrangement and packing through the film as it dries. A 1D model was proposed to predict the particle distribution through the coating thickness. However, limited researches exist to assess the conductive particles concentration gradients that develop during the drying process for organic system, while lots of polymer could only soluble in organic solution. In this regard, it is crucial to understand the processing-dependent particles transport behaviors in organic system. Recently, Fragouli *et al.*[27] obtained γ-Fe_2O_3/Fe_3O_4 nanowire arrays in an acrylate copolymer film during chloroform evaporation under external magnetic field. The dimensions and localization of the nanowires could be controlled by varying the evaporation dynamics and duration of magnetic field. Such approaches simplify the process, but the price of a wide range of homogeneous magnetic fields used for large-area fabrication so far have still been very high, limiting the broad application of such systems.

As a uniform, effective and common force filed, the earth's gravity field is more convenient than the other external force fields.[28–31] The conductive particles distribution may be controlled under gravity during solvent evaporation. Herein, Ni particles were selected as conductive filler due to their ferromagnetic nature and cheap price. This work is aimed to prepare high-performance EMI shielding thin films with a controllable Ni particles spatial configuration through a facile solution casting method. The rheological, evaporation behaviors of casting solution, sedimentation, dispersion state of Ni particles were systematically investigated. The mechanisms of the structure formation, through which conductive network contributed to the enhancement of electrical properties and EMI SE were also identified. An EMI SE up to 60 dB was achieved. Moreover, the obtained thin film exhibited excellent EMI SE values per unit film thickness of 200 dB/mm. The thermal conductivity of Ni/polyvinyl chloride (PVC) films was also explored. These advanced properties of such polymeric films allow their use as fundamental components in diverse devices.

EXPERIMENTAL

Materials

Commercial Ni particle (99.7 wt % purity) with an average primary particle size of 1.5 μm was supplied by Wuxi ShunDa Metal Particle Co., Ltd. PVC (SG-2) used in this work as a polymer matrix material was manufactured by Tianjin Letai Chem. Co. Tetrahydrofuran (THF, AR) used as the solvent was obtained from Beijing Chem. Co. Dioctyl phthalate plasticer (DOP) was purchased from QiLu Chemical Co. All the above materials were used as received.

Preparation of Ni/PVC Films

A series of Ni/PVC films was formulated by the following procedure. PVC resin was first dissolved in THF by using a mechanical stirrer. Secondly, DOP (W_{DOP} : W_{PVC} = 20 : 100) and Ni particles were added into the above solutions. The required amount of Ni particles was calculated based on the Ni particles volume fraction at 12 vol % (Ni particles vol % = volume of Ni particles /volume of resultant film × 100%). The solutions were homogenized for over 8 h under vigorous stirring to form the casting solution. Then, the desired amount of casting solution was immediately poured into a 30 cm × 30 cm × 2 cm evaporating dish. The evaporating dish was placed horizontally for 24 h under ambient conditions to allow the THF to evaporate. After that, the Ni/PVC films were removed from the evaporating dish and further dried in a vacuum oven at 30°C for more than 6 h to remove the residual solvent. The resultant films with the same thickness of 0.3 mm were obtained by varied the volume of casting solution. For final structure and properties studies, six different casting solutions, which containing 0.03, 0.06, 0.09, 0.105, 0.12, and 0.15 g/mL PVC, were prepared. The casting solutions are designated as S3 and so forth for the solutions containing 0.03 g/mL PVC and so forth, where the number indicates the initial PVC concentration. The specific dosages of all the chemical reagents for the casting solutions were listed in Table I. The resultant films are termed as F3 and so forth for the resultant films casted form solutions containing 0.03 g/mL PVC and so forth, where the number indicates the initial PVC concentration. The surface of the films exposure to air during the evaporation process was called the top surface, and the other side attached to evaporating dish was called the bottom surface.

Table I. The Specific Dosages of all the Chemical Reagents for the Casting Solutions

Casting solutions	Weight/g			Volume of THF/mL
	Ni particles	PVC	DOP	
S3	28.8	25.6	5.1	854
S6	28.8	25.6	5.1	427
S9	28.8	25.6	5.1	285
S10.5	28.8	25.6	5.1	244
S12	28.8	25.6	5.1	213
S15	28.8	25.6	5.1	170

Characterization

Viscosity measurements were performed with a rotational rheometer (Haake Mars III, Thermo Fisher Scientific). The shear rate was kept at 100 s^{-1} and the temperature was maintained constant at 20°C. A cylinder sensor system, Z41 DIN 53018 for the Haake rheometer was used. The thermogravimetric (TG) analysis were conducted on a TA TGA Q5000 (TA Instruments, Delaware, USA) from 40 to 650°C under nitrogen at a heating rate of 20°C·min $^{-1}$. The structures of films were examined using a FEI Quanta FEG 250 scanning electron microscope (SEM). Cross-sections of the films were cryo-fractured under liquid nitrogen to ensure brittle fracture. Before imaging, all the samples were sputter-coated with gold. Electrical resistivity measurements were conducted using two different instruments. For films with the surface resistivity above 10^6 ohm·cm, an EST-121 high resistance meter (Beijing Municipal Institute of Labor Protection, China) according to ASTM D257 was used. For films with surface resistivity lower than 10^6 ohm·cm, a four-point probes resistivity measurement system (Four Probes Tech, RTS-9, Guangzhou, China) was performed in order to eliminate the effect of contact resistance and the square resistance was obtained. Data of electrical resistivity were taken as averages of at least five measurements. By using the coaxial cable line test method based on ASTM D4935-10, the EMI shielding effectiveness was measured with an Agilent E5071C vector network analyzer (VNA) in a frequency range from 60 MHz to 1.5 GHz. A full two-port VNA calibration was performed at the beginning of each test sequence to correct systematic measurement errors. The thermal conductivity was determined using NETZSCH LFA 467 system by flash technique. Samples were coated with a very thin layer of graphite to improve emissivity and for uniform spreading of energy pulse through the sample. Pyroceram 9606 was chosen as the reference material. The thermal diffusivity and specific heat of each sample were measured at different temperatures from 30 to 60°C. The thermal conductivity was calculated by multiplying the thermal diffusivity, the heat capacity, and the density. At least five samples were tested and the average value was calculated.

RESULTS AND DISCUSSION

Rheological Properties of Casting Solution

The property of casting solution has a direct influence on particle transport,[26] which affected the resultant films structure. So the rheological properties of the casting solution were first studied. In addition, the PVC solutions with the same PVC concentration were also examined. Figure 1 shows the apparent viscosity versus various initial PVC concentrations. It was observed that the viscosity exponentially increased with the PVC concentration in both PVC and casting solutions. In addition, apparent viscosity of the casting solution is slightly higher than the PVC solution, especially for the solutions with high PVC concentration.

Ni Particles Motion-Evaporation *vs.* Sedimentation

Generally, evaporation, sedimentation and diffusion process determine the particle distributions during solution drying. Evaporation causes the coating free surface to descend toward the substrate. If the particles are denser than the surrounding medium, they have the tendency to form a "sediment" in the lower part of casting film. Thermal Brownian diffusion acts to eliminate particles accumulating effects and tends to create uniform concentration profiles. Sedimentation velocity is much higher than diffusion velocity for large and/or heavy particles.[32,33] The presence of PVC also slows the equilibrating diffusive motion of Ni particles. So transport of Ni particles is not significantly affected by Brownian diffusion and the Brownian diffusion motion is neglected in this study. In order to interpret the film-formation process, the evaporation rate and sedimentation velocity were investigated in details.

In the present work, the evaporation rate is termed as the velocity at which the coating surface descends toward to the evaporating dish. The plots of evaporation rate against time were presented in Figure 2. It can be observed that the dilute casting system (low initial PVC concentration) has the faster evaporation rate than that of the concentrated one (high initial PVC concentration) throughout the experimental time. Additionally, all the slope of curves drops with the time. In polymeric solutions, the evaporation rate depends on the solvent activity, which is proportional to solvent partial pressure adjacent to the surface of casting solution. The solvent partial pressure is affected by polymer concentration at top surface of the coating.[34] Therefore, the evaporation rate mainly hinges on polymer

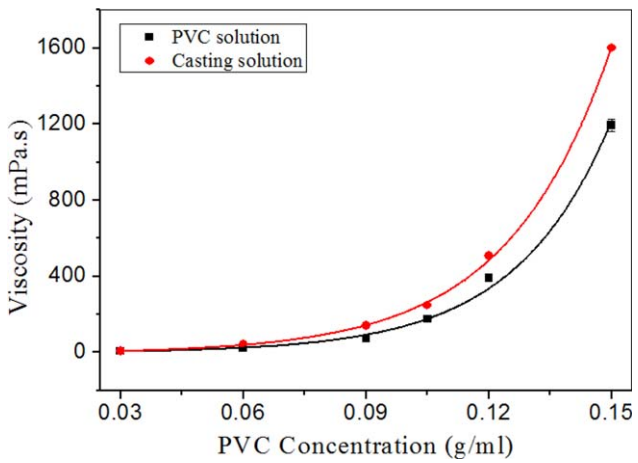

Figure 1. Relationship between the viscosity and solutions with various PVC concentrations. [Color figure can be viewed in the online issue, which is available at wileyonlinelibrary.com.]

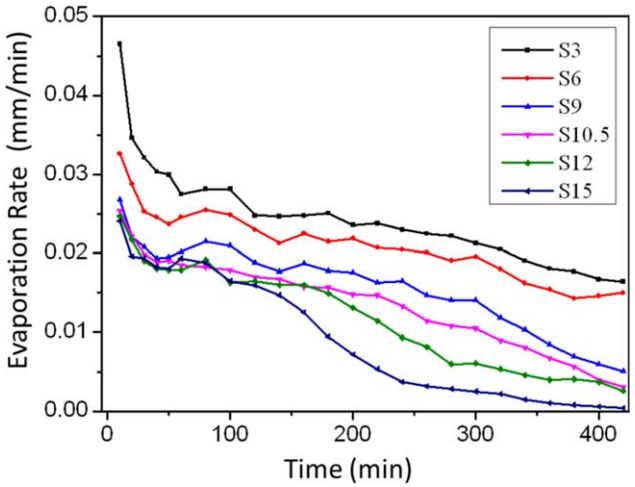

Figure 2. Dependence of the evaporation rate on time for various casting solutions. [Color figure can be viewed in the online issue, which is available at wileyonlinelibrary.com.]

concentration. So in this study, the evaporation rate for dilute casting systems (such as S3 and S6) is faster than that of the concentrated ones (such as S12 and S15), as shown in Figure 2. As drying continues and PVC concentration increases, the evaporation rate falls because the solvent activity decreased.[26]

The sedimentation behaviors of Ni particles also present the same tendency (Figure 3). For more precise measurements, a sample of each casting solution was poured into a test tube, then sealed and placed in static storage. The relative sedimentation height (RSH) was also examined. The RSH is defined as follows: RSH = (sediment cake height/entire casting solution height) × 100%. From Figure 3, it is obviously that the Ni particles experienced rapid sedimentation in dilute system. For example, almost all the Ni particles were settled down within 2 minutes for S3 and 4 minutes for S6. Meanwhile, the sedimentation was very slow for concentrated system. The Ni particles dispersion remained relatively well-dispersed during the first 1 h with only a small amount of sedimentation (5.1% for S15). After 24 h for almost all the Ni particles precipitated completely in all the solutions, the results showed that the RSH increases from 5% to 42% for the casting solutions from S3 to S15 (see Supporting Information Figure S1). It could be deduced that the concentrated solution showed better sedimentation stability than the dilute one. This is mostly due to the viscosity of casting solutions, which plays an important role by hindering severely the sedimentation velocity. The formation of Ni particle network is inhibited by PVC macromolecular network in concentrated system, resulting a high RSH. The PVC network cannot hold the Ni particles in the dilute system, so the Ni particles sink and pile up more regularly leading to a dense sediment near the substrate. The small RSH was obtained. By compared Figures 2 and 3, it is concluded that sedimentation velocity is much higher than evaporation rate for dilute system, which means that sedimentation overwhelms evaporation. The absolute velocity difference between evaporation and sedimentation becomes small for concentrated system as time progresses.

Spatial Configuration of Ni Particles in the Films

To compare the effectiveness of the Ni particles motion on the microstructure of the films, all the resultant films with the constant composition and the same thickness 0.3 mm were prepared. To confirm the content of Ni particles in films, TG analysis was performed. The TG curves of pristine PVC, DOP, and Ni/PVC films are shown in Figure 4. It was observed that the residual DOP mass was almost zero at 650°C. The Ni particles volume fraction in the films was estimated from TG results according to the following equations:

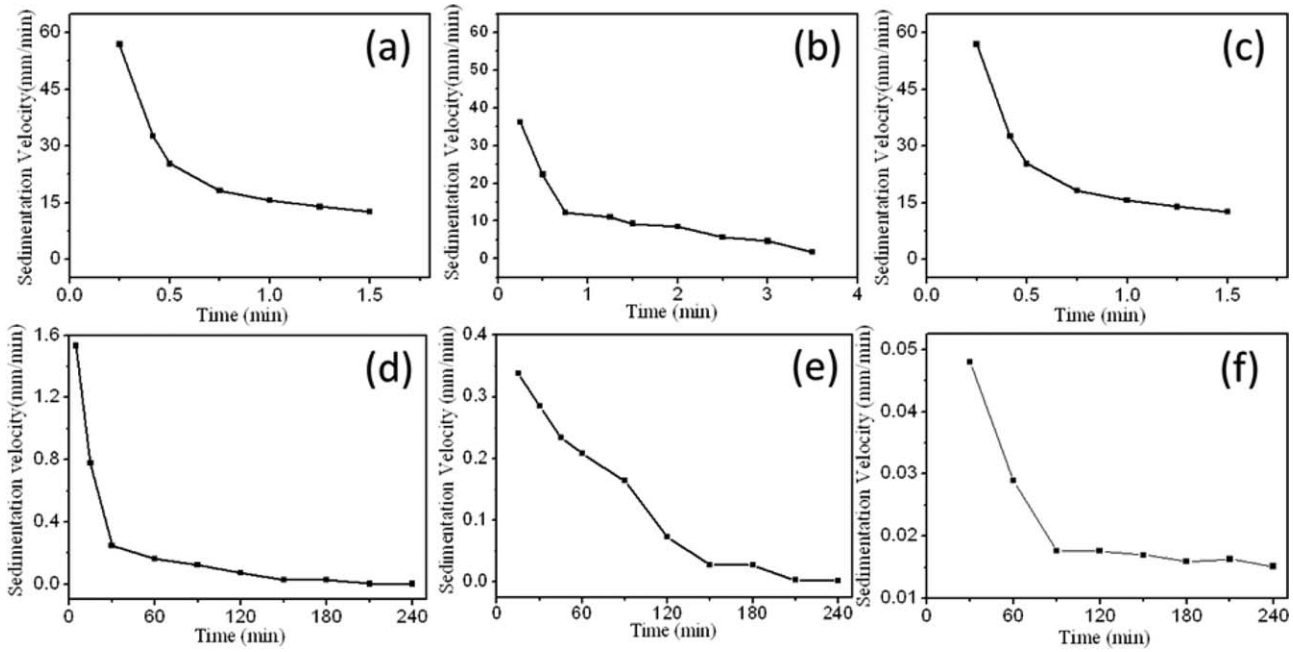

Figure 3. Relationship between the sedimentation velocity of Ni particles and time in various casting solutions. (a)∼(f) represent S3∼S15, respectively.

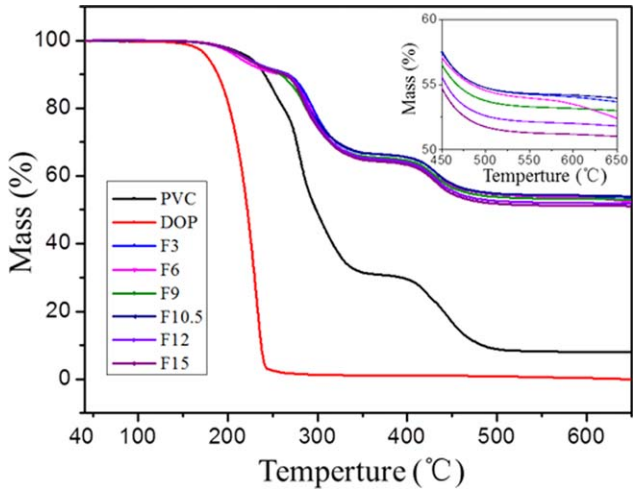

Figure 4. TG curves for the pristine PVC, DOP, and Ni/PVC films. The inset shows TG curves of Ni/PVC films from 450 to 650°C. [Color figure can be viewed in the online issue, which is available at wileyonlinelibrary.com.]

$$Ni\ particles\ \text{vol.}\% = \frac{M_{Ni}/\rho_{Ni}}{M_{PVC}/\rho_{PVC} + M_{DOP}/\rho_{DOP} + M_{Ni}/\rho_{Ni}} \times 100\% \quad (1)$$

$$Remaining\ mass\ wt.\% = \frac{0.081\ M_{PVC} + M_{Ni}}{M_{PVC} + M_{DOP} + M_{Ni}} \times 100\% \quad (2)$$

where M and ρ are the mass and density of components in films, respectively, and subscripts denote the components. 0.081 in eq. (2) was read from the pure PVC TG curve which was the pristine PVC remaining mass percent. According to the fabricating process, the mass ratio of DOP to PVC was 0.2. The TG results showed that the remaining mass fraction of films was around 52%. From the eqs. (1) and (2), it was calculated that the volume fraction of Ni particles was about 12 vol %. The weight percent of PVC, DOP, and Ni particles in the films was 43, 8.6, and 48.4 wt %, respectively.

A typical optical photograph of the Ni/PVC film is shown in Figure S2 (see Supporting Information). It was obvious that the obtained film showed a smooth surface and was quite flexible under bending. Figure 5(a∼i) show the representative SEM micrographs of cross-sectional morphologies of Ni/PVC films. Interestingly, different from the conductive fillers homogeneously dispersed in traditional polymer/conductive fillers composites, it could be observed that the number of Ni particles increased with the distance increasing from top to bottom surface along the thickness direction. So the Ni particles were asymmetrically distributed through the film. Based on the distribution of Ni particles, the film along the thickness direction can be mainly divided into two parts: upper and lower parts. Few Ni particles can be observed in the upper part, while a large number of Ni particles are seen in the lower part.

High-resolution SEM micrographs [Fig. 5(a∼c, g∼i)] reveal the structural details of the upper and lower parts. From Figure 5(a∼c), a Ni particle-free zone is found of each specimen, indicating that sedimentation has occurred. Less Ni particles embedded in PVC matrix for the upper part than that in the lower one. A careful examination of cross-sectional morphologies results indicates that the thickness of the Ni particle-free zone was varied. For example, the thickness of the particle-free zone is about 130 μm for F3, and this zone is decreased sharply to about 50 μm and 20 μm thick for F9 and F15, respectively.

The sedimentation overwhelms evaporation for dilute system, while the high viscosity slows both evaporation and sedimentation for concentrated system. Moreover, compared with concentrated system, the dilute system takes a long time to reach the same solution concentration, indicating a longer sedimentation time. Considering these transport parameters together, including evaporation rate, sedimentation velocity and time, the Ni particles concentration profiles to show a steeper transition slope from few particles at the top of the film to the maximum packing fraction near the substrate for the dilute casting system. The dense, closed Ni packing structure in the film lower part gradually decrease and the particle-free layer became thinner with the increase in viscosity.

This result is similar to calculations made by Cardinal and coworkers using the 1D model.[25] Results from the model are summarized in a dimensionless drying regime map. Regions on the map are defined where particles remain uniformly distributed or accumulate on the top surface, or in the lower part of the films. The axes of the map are two dimensionless numbers. One is the Peclet number (Pe), which describes the strength of evaporation to diffusion in a casting film of initial thickness H_0. It is given as

$$Pe = \frac{EH_0}{D_0} \quad (3)$$

where E is the evaporation rate and D_0 is the Stokes-Einstein diffusion coefficient. D_0 is defined as:

$$D_0 = \frac{KT}{6\pi\mu R} \quad (4)$$

for a spherical particle with the radius R dispersed in a liquid with viscosity μ and temperature T. The Botzmann constant is k. The other dimensionless number is the sedimentation number, N_s, which relates to the importance of sedimentation to evaporation:

$$N_s = \frac{U_0}{E} \quad (5)$$

where U_0 is the Stokes settling velocity.

At high Pe and low Ns casting system, where evaporation dominates, particles accumulate at the coating surface. Likewise, at high N_s, particles fall towards to the substrate faster than the free-surface descends, creating a particle-free zone. At low Pe and low N_s, the concentration profiles are uniform throughout the entire films since diffusion governs particles motion.

Because Stokes settling velocity is used for a single isolated particle in a dilute solution, so the actual particle sedimentation velocity (Uexp) was adopted instead of U_0 in eq. (5) to obtain the Ns, exp, as follows:

$$N_{s,exp} = \frac{U_{exp}}{E} \quad (6)$$

The Pe and $N_{s,exp}$ calculated based on eqs. (3) and (6), respectively. The results were summarized in Table II.

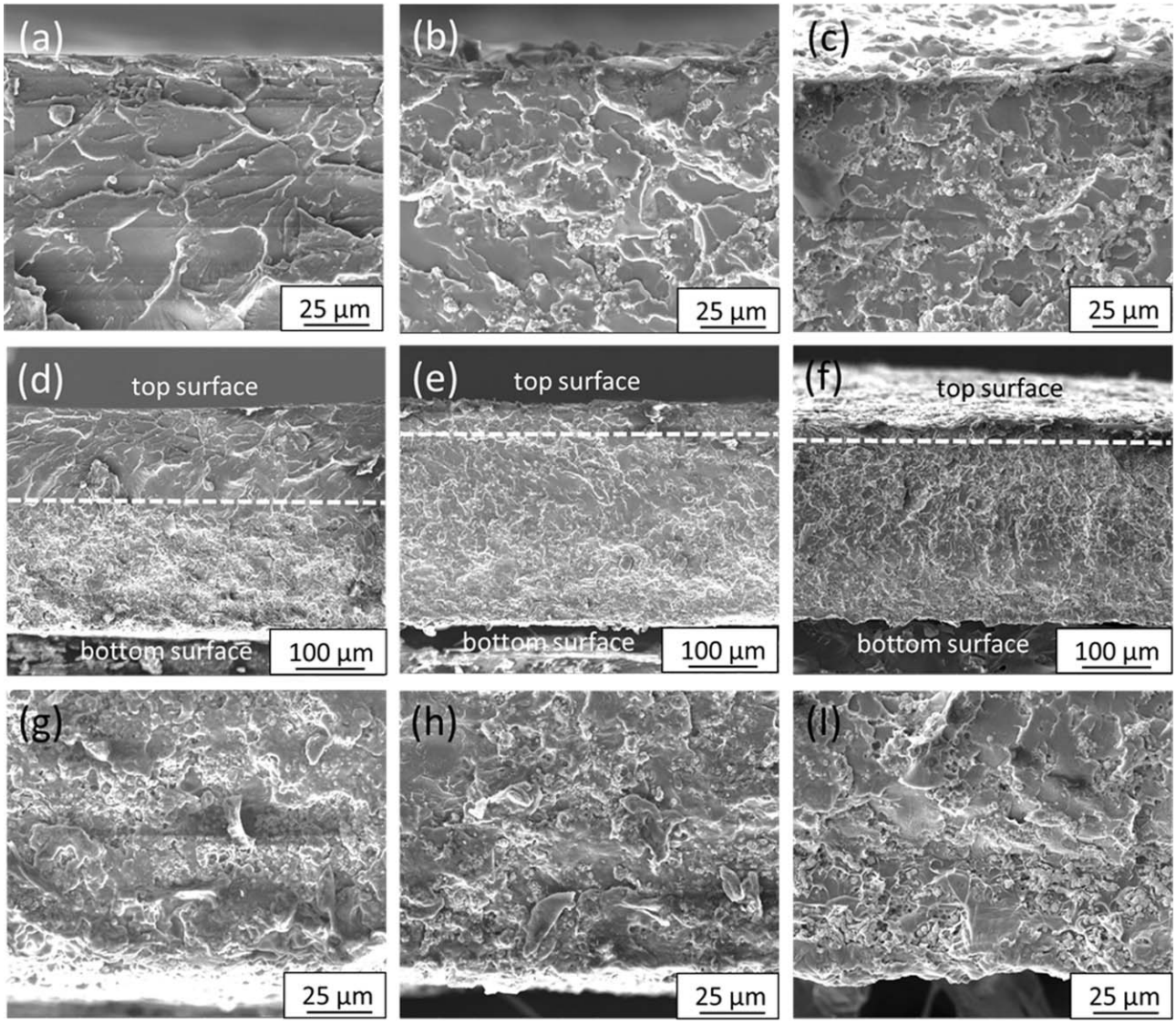

Figure 5. Cross-sectional SEM micrographs of (a), (d), (g) F3, (b), (e), (h) F9, and (c), (f), (i) F15. High magnification images of (a), (b), (c) upper part and (g), (h), (i) lower part of the Ni/PVC films. The white dashed line is labeled between upper and lower parts.

As shown in Table II, the *Pe* is much larger than 1, which means the effect of Ni particles diffusion can be ignored. At high $N_{s,exp}$, where sedimentation is stronger than evaporation, particles accumulate at the substrate and a particle-free zone appears at the top of the film [Figure 5(a)]. Decreasing the strength of sedimentation (decreasing $N_{s,exp}$) decreases the rate of particle accumulation in the lower part of the film by decreasing the thickness of the particle-free zone [Figure 5(c)]. So in this work, the experimental data fit the 1D model well.

According to above analyses and discussion, it could be confirmed that the competition between evaporation and diffusion determines the Ni particle concentration profile. A proposed mechanism for progressive evolution of the resultant film is illustrated in Figure 6. At the initial stage, the homogenous casting solution is casted into the evaporating dish. Then sedimentation occurs immediately for dilute system. Ni particles settled with a greater velocity than the evaporation velocity of the free surface, creating a region at the top of the casting film that was depleted of Ni particles. On the other hand, sedimentation is

Table II. *Pe* and $N_{s,exp}$ of Various Casting Solutions

Description	S3	S6	S9	S10.5	S12	S15
$Pe/10^5$	2.7	3.6	5.8	11.7	22.2	52.6
$N_{s,exp}$	1222.9	1110.7	120.1	60.5	13.7	2.0

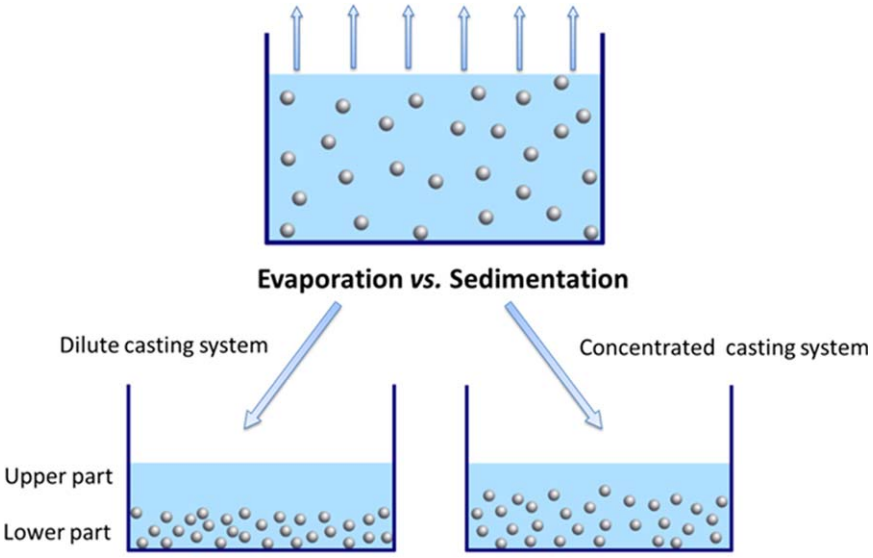

Figure 6. Schematic illustration of the formation of Ni/PVC films. [Color figure can be viewed in the online issue, which is available at wileyonlinelibrary.com.]

relatively slow for concentrated system. Fewer particles sink into the lower part of the casting film. The main effect of the soluble PVC is to raise the viscosity over the course of drying. As evaporation proceeds, the PVC concentration and solution viscosity become higher combined with the coating thickness shrinks. Both evaporation and sedimentation are slowed down. Ni particles motion is hindered to a greater extent. Finally, the entire casting film is at the maximum packing fraction and the dried particulate films with different thickness of particle-free zone are obtained.

Electrical Conductivity

Generally, the electrical properties of polymer/conductive fillers composites are mainly dependent on the dispersion of filler in the matrix because the polymer is an insulator. As stated early, Ni particles are asymmetric distributed in the film. A thorough conductive network and tunnel are not formed throughout the entire film. So the surface resistivity measurement was adopted instead of volume resistivity testing to evaluate the electrical conductivity of the films. Figure 7 illustrates the surface resistivity of Ni/PVC films. It is observed that the surface resistivity has great dependence on initial PVC concentration. For the films termed from F3 to F15, which were fabricated with increasing initial PVC concentration, the top surface resistivity decreases. A sharp decrease in resistivity from 4.8×10^{14} Ω for F3 to 1.1×10^{8} Ω for F9 was observed. Then it decreased slightly from 9.1×10^{7}Ω to 6.6×10^{7} Ω and 6.2×10^{7} Ω for F10.5, F12, and F15, respectively. This indicates that the top surface of Ni/PVC films is converted from insulator to semiconductor. The trend of the electric resistivity curve of bottom surface is quite different from that of the top surface. As can be seen in Figure 7(b), with increasing the initial PVC concentration, the surface resistivity of bottom surface increased gently from 0.3 Ω/square for F3 to 0.5 Ω/square for F9, and then it increased from 0.9 Ω/square for F10.5 to 2.5 Ω/square for F12, and finally reached 6.9 Ω/square for F15.

The bottom surface resistivity was much lower than the top one. Obviously, this interesting asymmetric phenomenon can be manifested from the special structure. In this study, the dispersion state of conductive Ni particles and the ease of formation of continuous conducting networks in PVC matrix are the two key factors which are responsible for the film conductive property. As discussed before, the concentration of Ni particles was

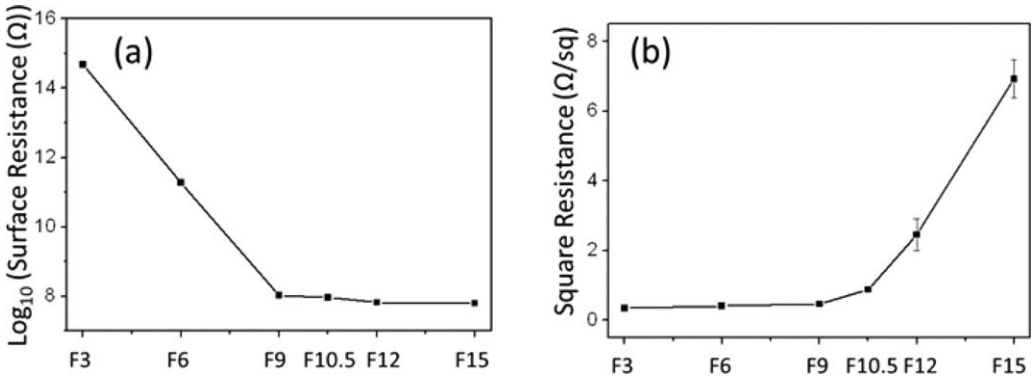

Figure 7. (a) Top and (b) bottom surface resistance of Ni/PVC films.

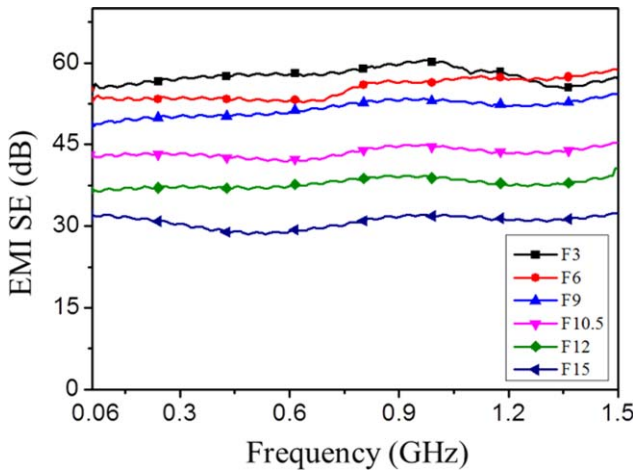

Figure 8. EMI SE as a function of frequency measured in the 60 MHz to 1.5 GHz range of asymmetric Ni/PVC films. [Color figure can be viewed in the online issue, which is available at wileyonlinelibrary.com.]

higher in the lower part than that of the upper part. There was a PVC-rich area between the two adjacent Ni particles in the film upper part. The electric charges cannot run across easily between PVC resin and the Ni particles. On the other side, lots of Ni particles were close to each other in the lower part, resulting in the contact points between Ni particles increased exponentially. This dispersion state of Ni particles makes it easy to form conductive networks penetrating throughout the surrounding PVC matrix. A more perfect conductive network was created, leading to a significantly improved surface conductivity. Moreover, the Ni particles in the upper part cannot connect up those in the lower part. So the top surface had lower conductive ability than the bottom surface. The top surface had extremely low electrical conductivity, while the bottom surface showed almost a conductor feature, especially for the films fabricated from the dilute casting system.

With increasing initial PVC concentration, the particle-free zone became thinner in the upper part. The existence of less conductive faults significantly increased the conductivity of the top surface, leading to a decrease of surface resistivity. For the lower part, sedimentation of Ni particles was inhibited by increasing the solution viscosity, resulting the content of Ni particles decreased in the lower part. So the bottom surface resistivity increased with the solution viscosity. Consequently, the special distribution of Ni particles indeed brings difference in the surface resistivity.

As is known to all, the EMI shielding performance of material depends on electrical conductivity property. It is worthy to mention that the remarkable enhancement of electrical conductivity potentially endows these asymmetric Ni/PVC films with good EMI shielding properties.

EMI Shielding Performance

The EMI shielding of Ni/PVC films was measured in a frequency range from 60 MHz to 1.5 GHz. Figure 8 shows the variation of EMI SE for Ni/PVC films. It is observed that almost all the films exhibited weak frequency dependency at the testing frequency, which indicates that these films have a broad bandwidth of shielding. The EMI SE of pure PVC film was also examined. The pure PVC film exhibited hardly any EMI SE due to its intrinsic electrical insulating characteristics. In contrast, the EMI SE was enhanced substantially after Ni particles filled PVC matrix. Hence it is clear that the major contribution to the EMI shielding comes from the Ni particle conductive networks. As shown in Figure 8, the EMI SE depends on the initial PVC concentration of the casting solutions. With increasing PVC concentration from 0.03 to 0.06, 0.09, 0.105, 0.12, and 0.15 g/mL, the SE decreases from 60 to 56, 53, 44, 38, and 32 dB, respectively. The film obtained from a low initial PVC concentration shows a remarkable high EMI SE.

To further confirm the enhancement of EMI SE induced by the special Ni particles distribution, three uniform films with equivalent Ni particles in the lower parts of asymmetric films F3, F9, and F15 were fabricated. These uniform films are denoted as FH3, FH9, and FH15, respectively. We assumed that the contents of Ni particles in the particle-free zone of asymmetric films could be neglected. The volume fraction of Ni particles in the lower parts of asymmetric films could be obtained by the following equations:

$$\mathrm{Ni_L\ vol\,\%} = \frac{m_{\mathrm{Ni}}/\rho_{\mathrm{Ni}}}{m_{\mathrm{L,PVC}}/\rho_{\mathrm{PVC}} + m_{\mathrm{L,DOP}}/\rho_{\mathrm{DOP}} + m_{\mathrm{Ni}}/\rho_{\mathrm{Ni}}} \times 100\% \quad (7)$$

The area of the films is the same on horizontal direction, so

$$\frac{V_{\mathrm{U}}}{V_{\mathrm{L}}} = \frac{h}{0.3-h} \quad (8)$$

$$V_{\mathrm{U}} = m_{\mathrm{U,PVC}}/\rho_{\mathrm{PVC}} + m_{\mathrm{U,\,DOP}}/\rho_{\mathrm{DOP}} \quad (9)$$

$$V_{\mathrm{L}} = m_{\mathrm{L,PVC}}/\rho_{\mathrm{PVC}} + m_{\mathrm{L,DOP}}/\rho_{\mathrm{DOP}} + m_{\mathrm{Ni}}/\rho_{\mathrm{Ni}} \quad (10)$$

where h is the thickness of the particle-free zone (the unit is mm), V is the film volume, and the subscripts U and L indicate upper and lower parts of the films. 0.3 in eq. (8) is the film thickness 0.3 mm. Based on the TG results in Figure 4, the mass ratio of Ni to PVC was 1.13.

According to eqs. (7) to (10), the volume fraction of Ni particles in the lower parts of F3, F9, and F15 is 22.6, 14.4, and

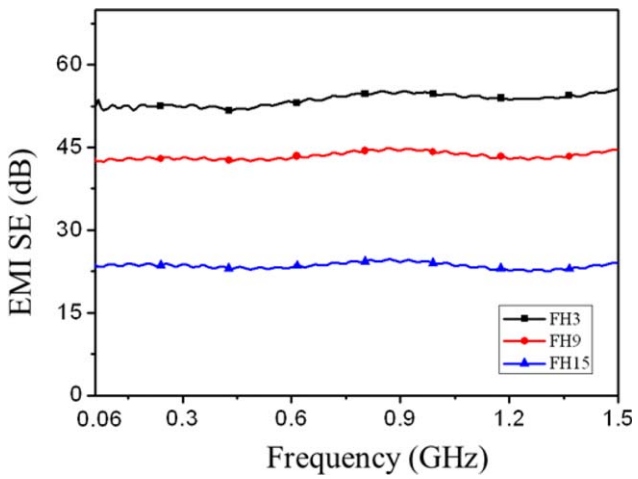

Figure 9. The variation of EMI SE for uniform Ni/PVC films. [Color figure can be viewed in the online issue, which is available at wileyonlinelibrary.com.]

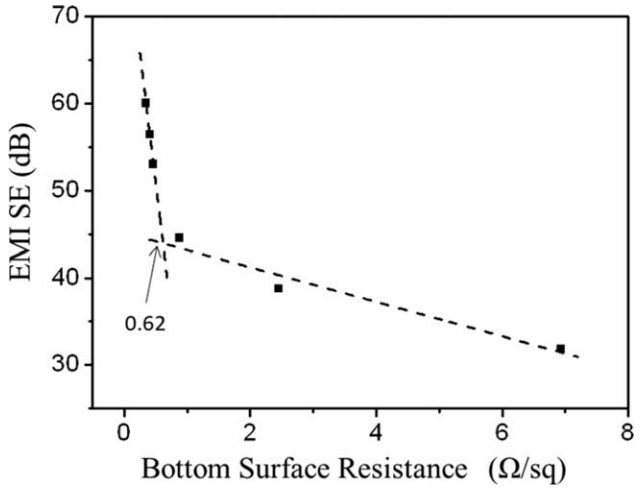

Figure 10. EMI SE as a function of bottom surface resistance at the fix frequency of 1.0 GHz.

12.9 vol %, respectively. The uniform films FH3, FH9, and FH15 were prepared with the corresponding Ni particles volume fraction by using 0.2 g/mL PVC solution. The thickness of all these uniform films was 0.3 mm. The cross-sectional morphologies of these uniform films are shown in Figure S3 (see Supporting Information). The electrical conductivity and EMI shielding performance were investigated. The surface resistance is 0.4, 0.9, and 8.3 Ω/ square for FH3, FH9, and FH15, respectively. The variation of EMI SE for these films was shown in Figure 9. Results show that the EMI SE is about 52, 43, 24 dB for FH3, FH9, and FH15, respectively. It could be concluded that the uniform films showed inferior shielding performance to the corresponding asymmetric films F3, F9, and F15.

This is attributed to spherical shape of Ni particles which is more difficult to make interactions between particles and particles in the uniform Ni/PVC film. In other words, much larger amount of Ni particles is needed for the uniform film to achieve the same shielding level as these asymmetric films. These data prove that the asymmetric structure has better ability in EMI shielding application. It is well know that, for commercial application that requires more than 20 dB of SE (i.e., equal to 1% transmission of the electromagnetic wave). Moreover, a SE of 30 dB, corresponding to 99.9% attenuation of the EMI radiation, is generally considered an adequate level of EMI shielding for many applications.[35] Thus, results in this paper indicate that all the asymmetric Ni/PVC films can meet the commercial application SE demands. Interestingly, about 60 dB SE could be achieved even at such a thin film thickness of 0.3 mm provides an added advantage. Thus make it an ideal candidate to reduce the size of complex electric equipment.

The composition and film thickness were kept the same for all the films. But the SE value of F3 shows two times as large as that of F15. The reason for the difference in EMI SE was mainly due to the special Ni particles distribution. A high effective dose of Ni particles in the film lower part results in the contact points between Ni particles increased in F3. The electron tunnels and conductive networks become perfect. So the number and the density of conducting networks are increased. The conducting networks present in this system acts as conductive mesh which intercepts electromagnetic radiation.[36] With the decrease in initial PVC concentration, the number of such conducting networks (mesh) increases in the path of electromagnetic radiation and the mesh size also decreases. The radiations those are not intercepted by the films obtained from the concentrated casting system and could be intercepted partly by the films obtained from the dilute casting system. Therefore, EMI SE

Table III. EMI SE of Various Solid Composites Measured at 1.0 GHz

Composite	Fillers content	EMI SE (dB)	Thickness (mm)	EMI SE values per unit thickness (dB/mm)
Heat-treated carbon nanofibers/LLDPE[36]	40 vol %	58	2.5	23.2
Heat-treated MWNT/LLDPE[36]	40 vol %	53	2.5	21.2
Reduced graphene oxide/PEI [37]	0.66 vol %	6.37	0.006	1061.7
Carbon fiber/PA66[38]	29.5 vol %	75	3.2	23.4
Wood's metal/PVC[39]	15 vol %	40	4.5	8.9
CNT-Ni/PUU[40]	7.4 wt %	4.3[a]	0.7	6.1
Vapor grown carbon nanofiber/HDPE[41]	7.5 vol %	30	2.0	15.0
0.4 μm Ni filaments/PES [42]	19 vol %	91.7	2.85	32.2
2 μm Ni fibers/PES [42]	19 vol %	71.1	2.85	24.9
20 μm Ni fibers/PES [42]	43 vol %	73.7	2.85	25.9
Carbon fiber/MWCNT/Polyester [43]	Carbon fiber : 46 vol %			
MWCNT : 0.34 vol %	78	1.16	67.2	
Ni/PVC (this work)	12 vol %	60.2	0.3	200.7

[a] Indicates that the value was measured at 1.3 GHz.

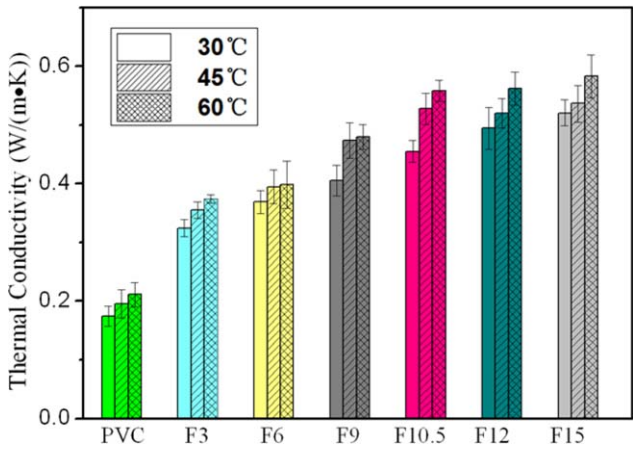

Figure 11. Thermal conductivity of PVC and asymmetric Ni/PVC films at 30, 45, and 60°C. [Color figure can be viewed in the online issue, which is available at wileyonlinelibrary.com.]

becomes higher. So the electromagnetic SE improves monotonically with decreasing initial PVC concentration. This leads to better shielding performance of the film.

The films exhibit 32∼60 dB EMI SE dependence on Ni particles distribution in this study. The dispersion state of conductive particles in polymeric matrix is reflected in electrical property. To better understand the effects of Ni particles spatial dispersion on EMI SE, we plotted EMI SE as a function of bottom surface resistance at the fix frequency of 1.0 GHz in Figure 10. In general, the EMI decreased with increasing bottom surface resistance. Somehow, the experimental data can be grouped into two linear regions with the two regression lines crossing at a value of 0.62 Ω/square for bottom surface resistance. This point lies between rapid and slowly increase in EMI SE, suggesting that much higher shielding performance could be achieved after surface resistivity below a certain value.

Because the SE is a strong function of material thickness and it is usually directly proportional with thickness, the EMI SE of various solid composites was divided by thickness to facilitate a more direct comparison. The EMI SE values per unit thickness reported by other researchers were summarized in Table III. It is seen that a dramatically higher EMI SE values per unit thickness (up to 200.7 dB/mm) is obtained for the present work, which is superior to those of most of the reported works. Although Kim *et al.*[37] obtained a higher EMI SE values per unit thickness in double-RGO/PEI film than that reported in this work due to a ultrathin film thickness of ∼ 6 μm, but the EMI SE is only 6.37 dB. Furthermore, lots of composites employed large filler contents and nanosized particles that are much more expensive than the Ni particles used in the current work.

Thermal Conductivity

From the above discussions, it can be concluded that these Ni/PVC films can be explored as EMI shielding materials. In addition, the heat-energy transfer issue is of fundamental importance in engineering design as well as for tailoring of thermal behavior of materials. Thermal conductivity is an important parameter for characterizing heat transfer performance of materials. The lower thermal conductivity is desirable when the purpose is to minimize heat losses, while the higher thermal conductivity is chosen in order to efficiently dissipate heat. Thus, the thermal conductivity of the Ni/PVC films was measured with laser flash technique at different temperatures. As shown in Figure 11, the pristine PVC film has a thermal conductivity of 0.17, 0.20, and 0.21 W/(m·K) at 30, 45 and 60°C, respectively. With the introduction of Ni particles, the thermal conductivity of Ni/PVC films tended to increase gradually to 0.32∼0.52 W/(m·K) at 30°C, 0.36∼0.54 W/(m·K) at 45°C, and 0.37∼0.58 W/(m·K) at 60°C, respectively. The thermal conductivity increases slightly with temperature. This behavior can be attributed to the interfacial thermal resistance between the Ni particles and PVC matrix. The interfacial thermal resistance decreases with increase in temperature.[38] This results in slightly higher thermal conductivity at higher temperature.

Meanwhile, a detailed examination of the results indicates that the thermal conductivity increases gradually for F3 to F15 at the same temperature. This result is intriguing because all the films have the same composition. It is well understood that the thermal conductive path of continuous Ni particles network is more effective than that of the PVC matrix due to the high intrinsic thermal conductivity of Ni. In this study, the continuous thermal transport pathways in the through-thickness direction may be blocked by the particle free zone, which acts as a barrier for thermal conduction. So the thickness of the particle free zone determines the thermal conductivity of the films. The thin particle free zone facilitates the pathway for conduction and heat transfer along the film thickness direction. On decreasing the thickness of particle free zone, there is a slight increase in the thermal conductivity.

CONCLUSIONS

In summary, the solution casting technology described here is a facile and scalable approach to prepare asymmetric Ni/PVC films with high-performance EMI shielding function. The Ni particles distribution in the films is dependent on the competition between evaporation and sedimentation during solvent evaporation. The structure of the resultant films can be controlled by adjusting the viscosity of the casting solutions. The distribution of Ni particles in the films fit the 1D model. This asymmetric structure plays a critical role in determining the electrical conductivity and EMI shielding functions. The obtained Ni/PVC films exhibited low bottom surface resistance and high EMI SE (up to 60 dB), which is an excellent performance at such a thin thickness (0.3 mm). This means the film presents excellent EMI SE values per unit film thickness (up to 200 dB/mm). The thermal conductivity depends on whether a Ni continuous network formation throughout the whole film in the temperature range of 30∼60°C. Furthermore, the free-standing Ni/PVC films are prepared with a nonchemical room-temperature process, combined with the advantages of a cheap and abundant supply of Ni particles, indicating that these films can be used commercially as high-performance shielding materials for electromagnetic radiation. Such knowledge would provide guidance for the design and preparation of novel thin, free-standing EMI shielding materials.

ACKNOWLEDGMENTS

This work was financially supported by the National Science Foundation of China (Grant Nos. 21274007, 51021064), the Project of Science and Technology Innovation Platform of Beijing Municipal Education Commission (PXM2012–014213-000025), and the Tribology Science Fund of State Key Laboratory of Tribology (SKLTKF12A10).

REFERENCES

1. Rohini, R.; Bose, S. *ACS Appl. Mat. Interfaces* **2014**, *6*, 11302.
2. Yang, Y.; Gupta, M. C.; Dudley, K. L.; Lawrence, R. W. *Adv. Mater.* **2005**, *17*, 1999.
3. Chang, J.; Liang, G.; Gu, A.; Cai, S.; Yuan, L. *Carbon* **2012**, *50*, 689.
4. Chen, Z.; Xu, C.; Ma, C.; Ren, W.; Cheng, H.-M. *Adv. Mater.* **2013**, *25*, 1296.
5. Pande, S.; Chaudhary, A.; Patel, D.; Singh, B. P.; Mathur, R. B. *RSC Adv.* **2014**, *4*, 13839.
6. Wang, J.; Zhou, H.; Zhuang, J.; Liu, Q. *Sci. Rep.* **2013**, *3*, 1.
7. Maiti, S.; Shrivastava, N. K.; Suin, S.; Khatua, B. B. *ACS Appl. Mat. Interfaces* **2013**, *5*, 4712.
8. Zhang, Y.; Fang, X.; Wen, B. *Chin. J. Polym. Sci.* **2015**, *33*, 899.
9. Thomassin, J.-M.; Lou, X.; Pagnoulle, C.; Saib, A.; Bednarz, L.; Huynen, I.; Jérôme, R.; Detrembleur, C. *J. Phys. Chem. C* **2007**, *111*, 11186.
10. Liu, Z.; Bai, G.; Huang, Y.; Ma, Y.; Du, F.; Li, F.; Guo, T.; Chen, Y. *Carbon* **2007**, *45*, 821.
11. Kumar, R.; Singh, A. P.; Chand, M.; Pant, R. P.; Kotnala, R. K.; Dhawan, S. K.; Mathur, R. B.; Dhakate, S. R. *RSC Adv.* **2014**, *4*, 23476.
12. Al-Saleh, M. H.; Sundararaj, U. *Carbon* **2009**, *47*, 1738.
13. Luechinger, N. A.; Booth, N.; Heness, G.; Bandyopadhyay, S.; Grass, R. N.; Stark, W. *J. Adv. Mater.* **2008**, *20*, 3044.
14. Zois, H.; Apekis, L.; Mamunya, Y. P. *J. Appl. Polym. Sci.* **2003**, *88*, 3013.
15. Kyrylyuk, A. V.; Hermant, M. C.; Schilling, T.; Klumperman, B.; Koning, C. E.; van der Schoot, P. *Nat. Nanotechnol.* **2011**, *6*, 364.
16. Kim, H.; Abdala, A. A.; Macosko, C. W. *Macromolecules* **2010**, *43*, 6515.
17. Ramanathan, T.; Stankovich, S.; Dikin, D. A.; Liu, H.; Shen, H.; Nguyen, S. T.; Brinson, L. C. *J. Polym. Sci. Polym. Phys.* **2007**, *45*, 2097.
18. Hu, M.; Gao, J.; Dong, Y.; Li, K.; Shan, G.; Yang, S.; Li, R. K.-Y. *Langmuir* **2012**, *28*, 7101.
19. Ji, K.; Zhao, H.; Zhang, J.; Chen, J.; Dai, Z. *Appl. Surf. Sci.* **2014**, *311*, 351.
20. Gao, W.; Shen, J.; Guo, S. *Polym. Eng. Sci.* **2014**, *54*, 1471.
21. Fragouli, D.; Das, A.; Innocenti, C.; Guttikonda, Y.; Rahman, S.; Liu, L.; Caramia, V.; Megaridis, C. M.; Athanassiou, A. *ACS Appl. Mat. Interfaces* **2014**, *6*, 4535.
22. Liang, J.; Wang, Y.; Huang, Y.; Ma, Y.; Liu, Z.; Cai, J.; Zhang, C.; Gao, H.; Chen, Y. *Carbon* **2009**, *47*, 922.
23. Kim, S.; Sung, J.; Ahn, K.; Lee, S. *Langmuir* **2009**, *25*, 6155.
24. Kim, S.; Hyun, K.; Kim, Y. S.; Struth, B.; Clasen, C.; Ahn, K. H. *Langmuir* **2013**, *29*, 10059.
25. Cardinal, C. M.; Jung, Y. D.; Ahn, K. H.; Francis, L. F. *Alche J.* **2010**, *56*, 2769.
26. Buss, F.; Roberts, C. C.; Crawford, K. S.; Peters, K.; Francis, L. F. *J. Colloid Interf. Sci.* **2011**, *359*, 112.
27. Fragouli, D.; Buonsanti, R.; Bertoni, G.; Sangregorio, C.; Innocenti, C.; Falqui, A.; Gatteschi, D.; Cozzoli, P. D.; Athanassiou, A.; Cingolani, R. *Acs Nano* **2010**, *4*, 1873.
28. Yoon, H.; Na, S.-H.; Choi, J.-Y.; Latthe, S. S.; Swihart, M. T.; Al-Deyab, S. S.; Yoon, S. S. *Langmuir* **2014**, *30*, 11761.
29. Tai, M. H.; Gao, P.; Tan, B. Y. L.; Sun, D. D.; Leckie, J. O. *ACS Appl. Mat. Interfaces* **2014**, *6*, 9393.
30. Kahrobaei, S.; Farajzadeh, R.; Suicmez, V. S.; Bruining, J. *Ind. Eng. Chem. Res.* **2012**, *51*, 14555.
31. Chen, G.; Hong, Y.; Walker, S. L. *Langmuir* **2009**, *26*, 314.
32. Cho, E. C.; Zhang, Q.; Xia, Y. *Nat. Nanotechnol.* **2011**, *6*, 385.
33. Upadhyay, R. V.; Laherisheth, Z.; Shah, K. *Smart Mater. Struct.* **2014**, *23*, 015002.
34. Cairncross, R. A.; Jeyadev, S.; Dunham, R. F.; Evans, K.; Francis, L. F.; Scriven, L. E. *J. Appl. Polym. Sci.* **1995**, *58*, 1279.
35. Yang, S. Y.; Lozano, K.; Lomeli, A.; Foltz, H. D.; Jones, R. *Compos. Part A* **2005**, *36*, 691.
36. Nayak, L.; Khastgir, D.; Chaki, T. K. *J. Mater. Sci.* **2013**, *48*, 1492.
37. Kim, S.; Oh, J.-S.; Kim, M.-G.; Jang, W.; Wang, M.; Kim, Y.; Seo, H. W.; Kim, Y. C.; Lee, J.-H.; Lee, Y.; Nam, J.-D. *ACS Appl. Mat. Interfaces* **2014**, *6*, 17647.
38. Jakubinek, M. B.; White, M. A.; Mu, M.; Winey, K. I. *Appl. Phys. Lett.* **2010**, *96*, 083105.